Blade Vibration: Some Key Elements in Design Verification

C. E. Danforth*
General Electric Company, Cincinnati, Ohio

From among the many topics in design verification of blade vibration, a crucial aspect of all air-breathing engines' qualification, this paper outlines in some detail two key considerations: 1) the assessment at a given operating point of compressor and fan blade vibration in relation to high-cycle fatigue; and 2) the identification of engine operating points worst for blade vibration. Discussion of these subjects, seemingly little treated in the literature, is presented in terms of an illustrative distillation of hitherto unpublished perspectives in blade stress, dynamics, and their experimental sensing as required for effective design and validation of modern blading.

A deliberate effort is made to illustrate design and design verification significance of blade dynamics, and increasingly three-dimensional stress distributions and levels as derived from precision experiments and massive numerical analysis investigations. For example, local time-average stresses three times elementary treatment levels, as generated by the interaction of blade twist, camber, and rim overhang, are indirectly capable of causing fatigue failures, attributable to nonexistent "mystery" vibration.

The effectiveness of design verification in extensive simulated flight tests can be enhanced by a systematic identification of operating conditions "worst" for blade vibration. Illustrative examples are given for blade vibration, both stable and self-excited.

Introduction

"PROVE your engine meets specification requirements." Elaborate experimental programs, ranging from laboratory component investigations to full engine demonstrations finally issuing in official qualification tests, are intended to supply appropriate proof. All engine characteristics are involved, from overall thrust through component aerothermodynamic efficiencies to structural element low cycle fatigue.

Blades require special emphasis in design and proof of adequacy, unusual among hardware parts in the range of technical areas encompassed by their design. Blades are the physical means of activating engine aerothermodynamic cycles. Aerodynamic design of their shapes govern the efficiency of the cycle; aeromechanical design of their vibration characteristics governs their freedom from metal fatigue and consequent durability. Aerodynamic and aeromechanical/vibration design are inextricably linked. Refinement in one area generally benefits the other: improved aerodynamic stage matching reduces flow separation and related blade excitation; blade vibration interpretation indicating excessive separation has led to an improved balance of aerodynamic loading among compressor stages. Since virtually all blade vibration is aerodynamically induced, and because aerodynamic design must employ experimental techniques for its own optimum refinement, the normal tendency for design and test to be independent aspects of engine development is largely replaced in the case of blade aeromechanical design by the practice of experimental verification and refinement as an integral part of the total design process.

From the many aspects of blade vibration design verification, this paper chooses to concentrate on two topics: an approach to assessing the acceptability of blading vibration relative to fatigue at a given operating point, and some considerations for recognizing operating points most important for assessment.

Deceptively simple, the first topic requires for fulfillment primarily a definition of blade dynamics and related, increasingly three-dimensional stress analysis. Vibration measurement is but the starting point. Inherently limited to providing samples of vibration intensity at a limited number of geometric locations, measurements—whether of strain or displacement—risk providing mere electronic decoration without interpretation. Blade fatigue is a point function depending upon time-average and vibratory stresses. Fatigue strength is not an overall blade design property nor is it indpendent of the operating conditions to which it is subjected. The essence of the assessment task is to relate a finite number of point measurements to the entire blade surface and support structure. Essential considerations in the following discussion, centered upon strain gage sensors will find, one expects, their counterpart even with the advent of more subtle sensing systems.

Within our experience, massive strain gage instrumentation of blading in the J79 development vehicle compressor marked the effective implementation of approaches outlined in this paper.[1] Meanwhile, advances in design verification refinement have reflected the increasing complexity of design more than changes in concept. Core compressors have advanced in stage loading and reflect associated higher Mach number aerodynamics in lower aspect ratio, relatively thinner blading subjected to increased centrifugal field stresses typified by tip speeds raised by 50%. Vibration primarily in the first two modes gave way to the need for assurance in complex panel modes. Increased air turning and airfoil camber give rise to stress fields more like those of shells than beams. Fans for high-flow design at high tip-speeds present stress and dynamics challenges muted, or absent, in the first all-instrumented core compressor. For a given radius ratio, blade root centrifugal pull has doubled. Stress for a given pull on the root section can double again locally because of three-dimensional stress fields, or "end effects," associated with high levels of built-in twist and camber. To "simple" blade modes must be added blade-shroud-disk system modes.

Received October 11, 1974; revision received March 14, 1975. The author gratefully acknowledges the opportunity afforded by the General Electric Company to write and publish this paper together with Company initiatives in, and support of, technology discussed in this paper. Long-standing collaboration of colleagues associated with this field is noted with appreciation.

Index categories: Airbreathing Engine Testing; Airbreathing Propulsion, Subsonic and Supersonic; Structural Dynamic Analysis.

*Chief Consulting Engineer—Aeromechanics; Group Engineering Division; Aircraft Engine Group. Associate Fellow AIAA.

Such design trends have required constant re-examination of fundamentals of, and advancement in, all blade-related areas: from the meaning of a simple Goodman diagram in light of high-cycle and low-cycle fatigue interaction and concentrations, through structural dynamics, to nonsteady aerodynamic excitations. In the light of high Mach flight and hostile environments such as crosswind operation of high bypass fans, it has become as important to pinpoint the worst operating points at which vibration severity is assessed (Sec. II) as is the process of assessment itself (Sec. I). The discussion emphasizes aerodynamically excited vibration, excluding for the present a number of specialized topics such as blade design for bird strike capability and vibration related thereto, as well as stall response.

In contrast with a sparse literature in this area which seemingly leaves the design significance of its technical challenges unrecognized or buried in the mathematics of numerical analysis, an overview is attempted here, concentrating on stress and dynamics aspects of blade vibration severity assessment considered to play a central role in stimulating necessary advances in several related areas: blade fatigue per se and related fracture mechanics, blade system dynamics optimization, numerical analysis development as related to three-dimensional stress analysis, as well as instrumentation, associated electronics an its data management.

I. Vibration Assessment for a Given Operating Point

Assessment of blade vibration severity relative to fatigue consists of: 1) sensing for a given mode of vibration, the amplitude and frequency of vibratory stress at a limited number of points on the blade surface; 2) deducing from that particular reference vibratory stress the point on the blade for which the margin of its vibratory stress is least with respect to its local fatigue endurance; 3) infering such fatigue margin for the most active blade in the given cascade; and 4) establishing the corresponding margin in the case of multiple-mode response.

Stress Range Diagram and Critical Point Definition

For simplicity, let us ignore complexities of fatigue strength as a function of time-frequency relations, creep, and interaction of high-cycle and low-cycle fatigue, so that effectively unlimited cyclic life may be represented in the familiar form of stress range diagrams such as the schematic in Fig. 1. Curve "C_1" represents the upper bound of alternating stress for unlimited life vs mean stress as given for statistically "minimum" properties. Curve "C_1" reflects undamaged material, manufactured according to prescribed blade surface preparation and without concentration. Curve "C_2" represents blade fatigue strength in terms of nominal stress in the presence of a notch (whether of design geometry, foreign-object damage (FOD) induced, or a notch-equivalent degradation induced by instrumentation surface preparation for test vehicles). The level and shape of curve "C_2" relative to curve "C_1" depends on the severity of the notch concentration—the higher the concentration, the lower and more concave is curve "C_2". Curve "C_3" is, in a sense, the limiting case of the curve "C_2" family. It represents the upper bound of alternating stress consistent with crack propagation avoidance, a level of significance for blade durability in the presence of extreme FOD.

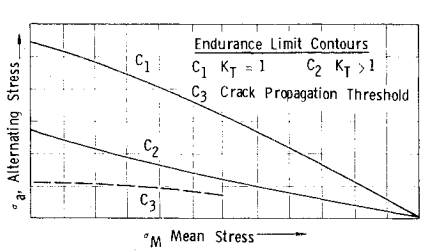

Fig. 1 Schematic of typical stress range diagram.

To establish a reference measure of vibratory stress severity directly applicable in development investigation and independent of the wide range of possible, in-service FOD concentrations, local vibratory stress may be expressed in "percent endurance" referred to curve C_1. Thus, for vibratory stress, σ_{v1}, in presence of mean stress, σ_{m1}, and an associated endurance stress, σ_{a1},

$$\text{Percent Endurance} = 100 \times \sigma_{v1}/\sigma_{a1}$$

Alternatively,

$$\text{Percent Crack Propagation Level} = 100 \times \sigma_{v1}/\sigma_{c1}$$

An exception of ranking the severity of vibration in terms of percent endurance is blade vibration associated with blade instability or "flutter." Very special situations apart, one does not distinguish among degrees of observed flutter severity. Rather, one must assure operational margins by which blade flutter in a given fan or compressor is avoided for all actual operational conditions in a specific application.

Fatigue Critical Point Definition

It is a natural temptation both in design and in fatigue margin assessment to consider vibration as limited, in the sense of a stress range diagram, by conditions obtaining at the geometric point experiencing highest vibratory stress. Generally false for a pure mode response, this misconception is magnified for simultaneous response in two or more modes.

Consider a tapered rotor blade, idealized to be without twist or end effect stresses, executing vibration in the second flexural mode, the highest vibratory stress at any spanwise section being at the maximum thickness point of the convex surface. Vibratory and mean centrifugal stresses are a function of spanwise position and tip amplitude alone. In Fig. 2 the spanwise distributions of mean and vibratory stress are shown together with their point-by-point transfer to the stress range diagram of Fig. 2b. Vibratory amplitudes have been adjusted so that the peak vibratory stress coincides with the endurance limit envelope at Point "A." The locus of mean and vibratory stresses traces the path "C" in the stress range diagram. If judged by the peak vibratory stress point, the blade is not over the fatigue limit. But point "B" exceeds the limit. The blade will fail. The tip amplitude must be limited so that point "B," the root section with higher mean stress and lower vibratory stress, does not exceed the endurance limit. Now the limiting distribution of vibratory stress ac-

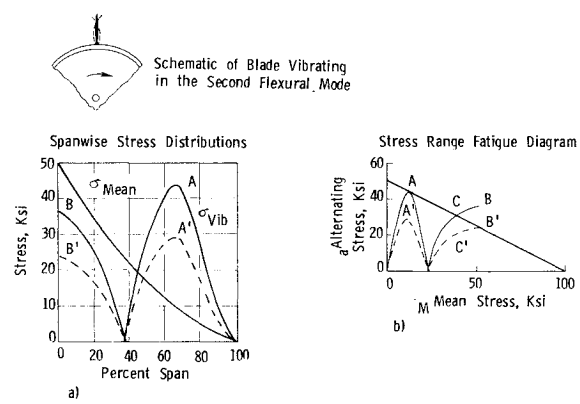

Fig. 2 Fatigue critical point relationships.

cording to which the blade as a whole vibrates at 100% endurance is traced by path C′ with B′ the "critical point." Note that while vibration at point "A" was only 22% higher than at point "B", the level of vibration had to be depressed by 33%. More easily stated than applied in complex geometries, the simple critical point concept merits constant re-examination to avoid oversights in fatigue assessment. To express it more generally, the entire blade structural system must be examined in a similar manner; e.g., the airfoil itself, its part-span shroud (denoted elsewhere variously as snubbers, clappers, dampers, or "wings"), and support attachment.

It follows that the level of vibration can be expressed in percent endurance in the case of multiple-mode response as the sum of the percent endurance levels for pure modes, taken separately, only if they have a common critical point. In general, the percent endurance for the blade, whether taken as a whole, or examined specifically at the FOD-prone leading edge, is less in the case of multiple mode response than the linear sum of percent endurance for the modes taken separately.

In multiple-mode response, the critical point is generally distinct from the critical point of any of the component modes taken separately; indeed it is also a function of the relative amplitudes among the modes constituting the combined response. Numerical definition for reasonably restricted conditions has been given in an earlier paper.[2] Illustrative trends relevant to variables above are now discussed.

Mean Stress Definition

Fan blade root section centrifugal field stresses, locally as high as two or three times nominal stress levels associated with direct pull and net cross-sectional area, provide a perspective that more is involved in modern blade mean stress definition as a basis for fatigue assessment than might be suggested by elementary beam theory. Without adequate definition of such mean stress peaks, one might well attribute certain types of fatigue to a nonexistent "mystery" vibration rather than to actual depression of endurance strength in the sense of a stress range diagram.

Anticipation of complex geometry stresses by inference from swept wing studies, together with a seemingly improbable carryover from mathematical treatments of "end effects" in radio frequency wave guides, has permitted keeping pace with practical implications of "end effect" stresses at airfoil termination zones—root section, shroud junctions—where stress fields are increasingly three-dimensional as radius ratio drops while tip speed rises and both root camber and built-in twist escalate. In principle, no mystery of physics is involved in "end effect" stress definition. One merely has to solve the classical equations of elasticity. Practical challenges arise, however, for their expeditious and reliable solution for arbitrary geometries, whether one invokes photoelastic techniques not readily applicable for mode-dependent dynamic counterparts of time-average stress, or techniques of numerical analysis, the latter having provided us with important specifics of vibratory mode definition in low-aspect ratio and composite blading.[3]

Design insights and related tradeoff options, as well as directly useful data, may be derived from treating airfoils in zones removed from three-dimensional junctions by theory already adequate and applying associated pure pull, moment, and torque loads to junction zones (root, shroud termination zones) in the manner of "black box" transfer functions—a combination of analysis and precision laboratory experiment. Long employed in our experience, such formulations were mandatory before comparatively recent three-dimensional analysis techniques became available, and are still powerful tools. Examples of

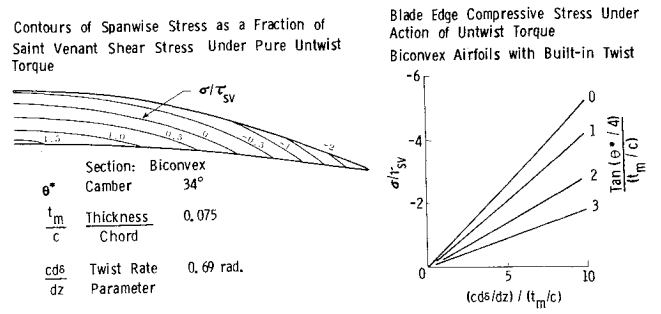

Fig. 3 Pure torque loads induce significant spanwise stress in cambered airfoils with built-in twist.

deviation from elementary stress analysis are relevant to this discussion.

Torque-Generated Spanwise Stress

Under the action of a pure torque vector along their spanwise direction, even far from termination zones, airfoils experience spanwise stresses which become increasingly important the larger the section camber and built-in twist rate. For blades without built-in twist and camber, torque generates simple shear stress in the classical manner of Saint Venant. The readily computed Saint Venant shear stress provides a convenient base for expressing spanwise stress torque generated in twisted and cambered airfoils, strictly speaking, without taper or change in cross section or built-in twist "far" from terminations. By an extension of the twisted bar formulation of Chen Chu[4] to include camber, an early survey was obtained for the significance of twist and camber-dependent torsional stiffness and spanwise stress. Figure 3 shows at the left spanwise stress contours over the biconvex section of an airfoil of high built-in twist for the case that the direction of torque serves to reduce built-in twist, as in the case of a cantilever rotor blade untwisting in the centrifugal field. Edges experience a compressive stress component as does the maximum thickness point of the convex surface, while the midchord, concave surface undergoes a tensile stress. In cantilever blade untwist at high rotor speed, blade edges experience spanwise stress lower than that of the direct pull P/A stress; the midchord concave point, a higher than P/A stress. This tendency is carried over into blade termination zones, e.g., at the root platform. For biconvex airfoils subjected to untwist torque—and free from restraint of lateral displacements which must coexist with torque application in such geometries—a calibration survey is presented in Fig. 3 for edge compression in multiples of Saint Venant shear stress as a function of camber, peak thickness-to-chord ratio, t_m/c, and the nondimensional twist rate parameter. This last variable is the product of chord length and twist gradient, in radians per unit spanwise length.

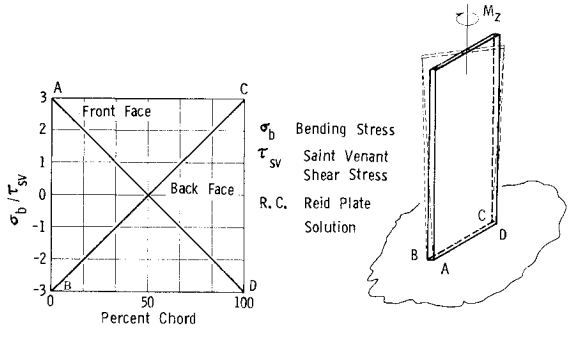

Fig. 4 Illustrative elementary end effect stress. Bending at root of cantilever bar in torsion.

At airfoil junctions, more complex spanwise stresses are generated by a pure torque moment. Edges at blade roots undergo bending, as one immediately perceives, even for the case of no camber or built-in twist. For example, edges of a rectangular bar terminated by a rigid surface normal to its spanwise axis experience a spanwise bending stress, σ_b, of magnitude 2.9 times the Saint Venant reference shear stress, τ_{sv}. This is one of the simplest cases of "end effect" stresses. Levels of edge bending stress, σ_b/τ_{sv}, in actual airfoils even of fairly arbitrary geometry are generally bounded by the classical bar case shown in Fig. 4.

Pull End Effect With Partial-Chord Dovetail

Because any excess blade weight increment pyramids through rotor and static structures, disk rim optimization frequently permits a rotor blade to be supported by a dovetail of axial depth less than the blade root chord. Blade centrifugal pull tends to concentrate centrifugal stress over that portion of the blade root chord directly above the partial-chord dovetail. Even without high built-in twist rates or camber, airfoils thus supported experience root pull load stresses significantly above their normal-level chordwise distribution and may be skewed to the extent that overhung trailing edges experience compression. Figure 5 shows a stress distribution of the type one might expect at the root of the blade supported in the manner described.

End Effect With Large Twist Gradient and Camber

An analogous mechanism is at work at blade root sections even with full chord support for airfoils of extreme twist rate parameter and high levels of camber. Radial stack-up of sections in such blades results in the visual appearance of trailing-edge "bowing." Viewed from the aft side, the trailing edge joins the platform at an appreciable angle deviation,in the counter-rotation direction, from the radial spanwise direction. As in the case of partial chord support, such "bowing" provides load paths for spanwise pull which concentrate the load in the forward portion of the airfoil. The greater the built-in twist rate, the greater is this effect giving rise to forward section tensile stresses far over the P/A level, together with compressive trailing-edge stresses. Studies have shown that in the presence of high levels of camber peak pull load stresses can rise to over three times nominal P/A stress as the built-in twist parameter approaches the value 1.5, while trailing-edge stress becomes numerically almost as high but in compression.

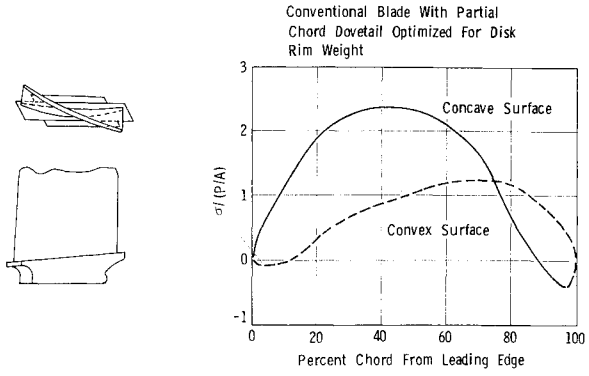

Fig. 5 Illustrative end effects stress. Blade root in spanwise pull compared to nominal pull/area stress.

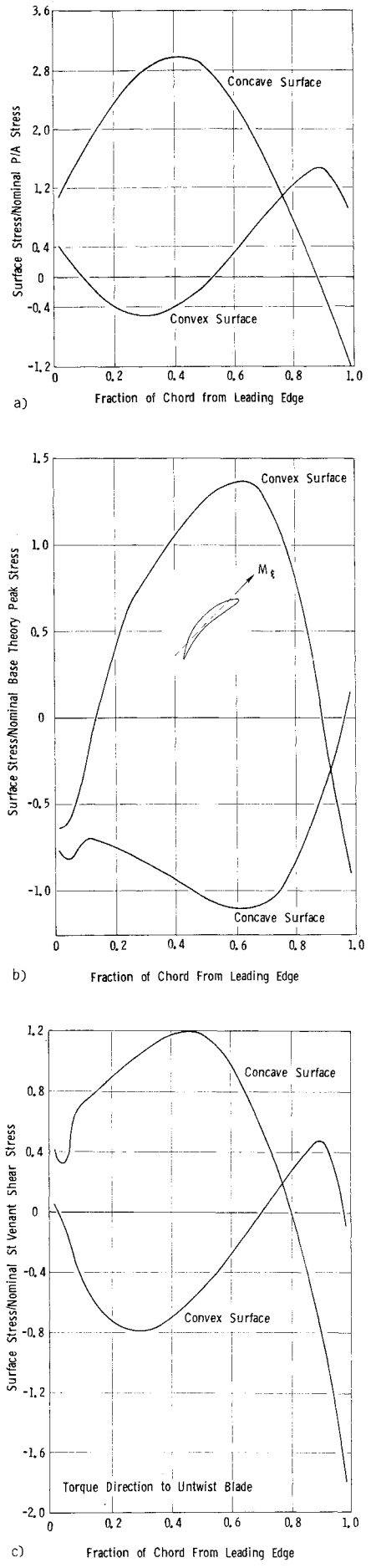

Fig. 6 End effect stresses for illustrative fan blade root section: a) Spanwise pull, b) moment, and c) torque load.

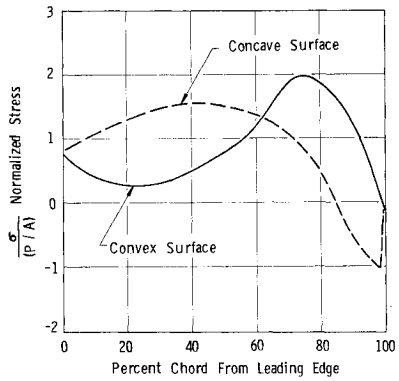

Fig. 7 Hypothetical fan blade root mean stress distribution normalized to nominal centrifugal stress.

Blade Root End Effect Stresses—Normalized Unit Load Distributions

Operational fan blades experience root section stress distributions deviating from simple beam theory definition by both the preceding considerations of geometry, built-in twist, and the assembly of parameters associated with their mounting: platform slope resulting from flowpath convergence and analogous to wing sweepback, some degree of edge overhang beyond in-line dovetail support, and the general transition profile between airfoil root section and the dovetail.

For one range of fan-blade design, stress distributions around the root section periphery are shown in Fig. 6 where loading is that of a pure pull load, the radial component of the centrifugal field, a pure twisting moment, and a pure bending moment about the nominal least moment of inertia axis. Stress magnitudes are normalized with respect to their respective beam theory counterparts.

Resultant Root Section Mean Stresses: An Illustrative Distribution.

Useful for design refinement though it is to sort out end effect stresses resulting from each component load, only their combined resultant is relevant in computing mean stress as a basis for fatigue assessment. Simplifying for illustrative purposes as if only spanwise stress were significant, we may superpose component load stress/load transfer functions point by point in the form:

$$\sigma_{ik} = \left(\frac{\sigma A}{F}\right)_i \left(\frac{F}{A}\right)_k + \left(\frac{\sigma c^3}{M_x}\right)_i \left(\frac{M_x}{c^3}\right)_k + \left(\frac{\sigma c^3}{M_y}\right)_i \left(\frac{M_y}{c^3}\right)_k + \left(\frac{\sigma c^3}{M_z}\right)_i \left(\frac{M_z}{c^3}\right)_k \quad (1)$$

where "i" designates the geometric grid point studied, "A" is cross-sectional area, "F" is spanwise pull, "C" is chord, and "M" is the moment vector applied in the x, y, z directions, respectively, the rotation, axial, and radial directions; and k denotes the operating condition.

Figure 7 presents the resultant mean stress distribution of a fanblade root section where stress magnitudes are normalized with respect to the simple "P/A" stress corresponding to the gross variables of centrifugal field radial pull, "P," and net root cross-sectional area, "A." This distribution will be used as a reference base for obtaining an illustrative measure of the significance of end effect stress distributions as they affect fatigue severity assessments which might be drawn from elementary beam theory. It should be noted that this stress distribution and its implied magnitudes apply to no known specific design. Magnitudes reflect a range of design studies, neither the highest nor the lowest. General characteristics such as trailing-edge compression and normalized concave surface stress above unity, between leading edge and midchord, are fairly typical. Peak tensile stress need not invariably occur near the trailing edge nor even on the convex surface. Its location depends on the interaction of camber, sweepback, twist rate, and blade mounting variables already noted as they apply in a given design. Rather, Fig. 7 is intended to indicate the arbitrary and highly nonuniform character of fan-blade root mean stresses and to give some hint of their magnitudes. In fans, such resultant mean stress distributions are largely dominated by centrifugal field loads, and secondarily, by air loads distributed over the airfoil.

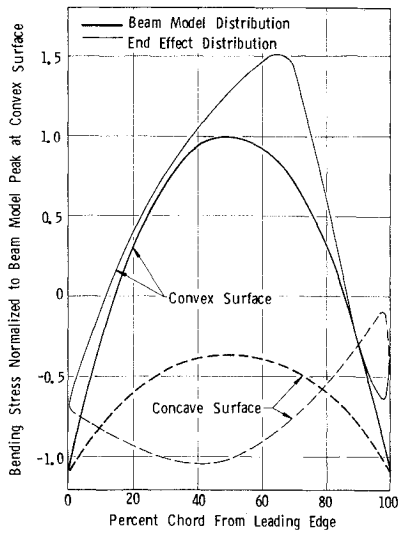

Fig. 8 Blade root bending stress for moment about least moment of inertia axis.

Allowable Vibratory Stress Levels—A Simple Case

Consider the limiting case that vibratory stresses at a fan blade root section are solely those generated by a vibratory moment about the nominal least moment of inertia axis. Actually impossible for a realistically twisted, cambered airfoil, this loading might be approached in the case of a cantilever blade vibrating in its first flexural mode.

Blade limiting vibratory amplitude as determined by stress distributions with end effects taken into account, will be compared with fatigue limiting vibration as determined by elementary nominal stresses. (It is assumed that prior analysis has already established that the fatigue critical point for this mode is at the blade root periphery).

Figure 8 presents an overlay of root section bending stresses including end effects together with the corresponding beam theory distributions, both normalized to the beam theory stress peak on the convex midchord sur-

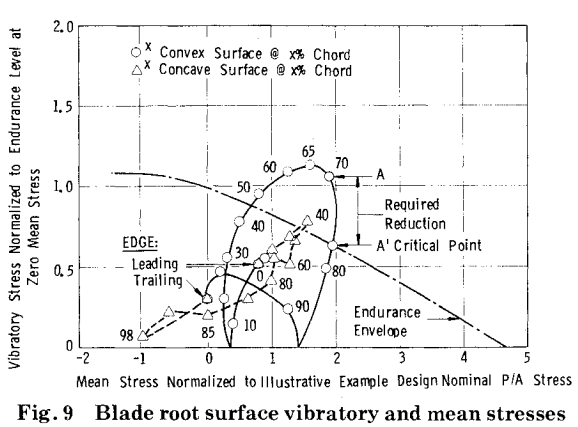

Fig. 9 Blade root surface vibratory and mean stresses

face. Fairly common end effect characteristics are noted: the stress loop at the trailing edge; the convex surface stress peaking above the nominal level; and concave surface levels considerably above their nominal counterparts. This vibratory stress distribution will be considered in the context of the mean stress distribution shown in Fig. 7. To determine the fatigue critical point, we transfer consistent combinations of mean and vibratory stress to a fatigue stress range diagram, point-by-point around the blade root periphery. To permit our concentrating on significant relationships rather than absolute levels of stress, a normalized fatigue stress range diagram has been constructed in Fig. 9. Mean stress has been normalized to the blade root steady stress defined without benefit of end effect stresses; indeed, on the basis that mean stress is simply the radial pull stress, P/A; air load stresses being negligible or otherwise canceled. Vibratory stress is normalized to the fatigue endurance limit for zero mean stress. Against these normalized coordinates is plotted a reference fatigue endurance envelope, a statistical minimum, effectively consistent with infinite vibratory cycle life under material/temperature combinations from which creep is absent.

According to the stress range diagram shown, allowable vibratory stress for the nominal (P/A) mean stress is 82% of the zero mean stress endurance level.

To obtain an indication of error in establishing blade allowable vibratory amplitude incurred by omitting reference to end effect stresses, assume that allowable vibratory amplitude is set by equating beam theory edge stress with vibratory stress allowable for the "P/A" nominal mean stress. With this reference, we transfer to Fig. 9 selected surface point mean stress levels from Fig. 7, together with corresponding vibratory stress levels with end effects included as given in Fig. 8. Circles refer to the convex surface; triangles, concave surface. Superscripts denote surface point location in percent chord from the leading edge.

Clearly the blade edges are not fatigue-critical points as the most elementary stress model would indicate, but rather the convex surface point at 70% chord with actual vibration at level A. For its local mean stress, it is farthest above the corresponding point on the endurance envelope. This vibratory stress level must be reduced to level A′. In this case elementary analysis would permit vibration in excess of that for unlimited fatigue life by 65%. Parenthetically, one observes that the critical point is not that for peak vibratory stress. Vibratory stress at 65% chord is higher by 7%, an almost trivial illustration of more pronounced divergences common between critical point and peak vibratory stress point.

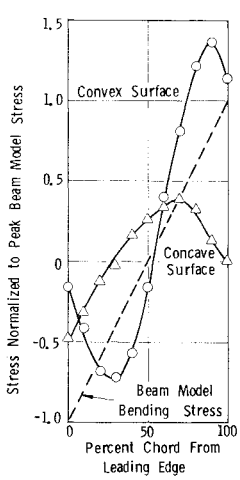

Fig. 10 Blade root relative stress for moment about maximum moment of inertia axis.

Consideration of Blade Root Fatigue in a Combined-Moment Mode

A simple extension of the preceding illustration permits a consideration of a more realistic and only slightly more complicated mode of vibration: one which involves blade root section vibratory moments about both nominal principal axes. Differences will be noted in critical point location, amplitude of vibration permitted, and the sensing of that vibration as affected by the divergence between elementary theory stress distributions and those including end effect stresses.

Illustrative trends for blade surface stress distribution and their normalized magnitudes are given in Fig. 10 for a bending moment, M_η, about the section nominal maximum moment of inertia axis. One observes a fairly common indication of bending in the direction normal to that expected for the moment M_η, a convex trailing-edge stress in excess of elementary analysis levels, and lower than elementary analysis levels at the leading edge.

In what follows, we assume vibration in which both M_ζ, bending about the least moment of inertia axis, and M_η are present. Further, we assume that peak stresses as evaluated by elementary theory for these two moments bear the relation: $(\sigma/M_\eta)/(\sigma/M_\zeta) = 0.16$, an arbitrary selection, not critically affecting trends to be considered. Elementary analysis yields combined moment stress distributions for the convex surface as shown in Fig. 11. All stresses are normalized to the midchord convex stress level as evaluated by elementary analysis and consistentwith Fig. 8. By far the highest vibratory stress is found at the leading edge and nearly doubles in magnitude as the ratio M_η/M_ζ increases in the range shown $0 \leq M_\eta/M_\zeta \leq 6$.

In contrast, end effect stress distributions for the same range of combined moments are shown in Fig. 12. Distributions differ markedly from those of elementary analysis: leading-edge stress increases only 24% in the same range of increasing M_η/M_ζ, while near midchord, stress rises by 45%.

Examining end effect vibratory and mean stress distributions concurrently in the context of Fig. 9, one finds that the fatigue critical point is located on the convex surface at 70% of the chord aft of the leading edge for the full range $0 \leq M_\eta/M_\zeta \leq 6$.

And if one compares levels of permissible vibratory amplitude in the manner done for the case of M_ζ applied

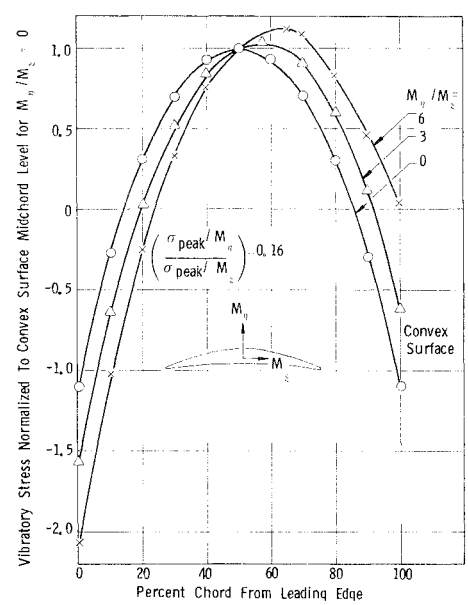

Fig. 11 Blade surface stress distribution—a function of bending moment ratio. Beam model.

alone, one finds that elementary analysis yields vibration excessive compared to that indicated by realistic end effect stresses. Specifically, if one presumes that by elementary stress distributions allowable vibratory amplitude would be set by leading-edge vibratory stress and a nominal P/A mean stress, then the actual end effect stress distributions would lead to the conclusion that vibration is excessive by these amounts:

M_η/M_ξ	0	3	6
Percent excessive vibration due to elementary approach	65	38	34.5

But if we limit vibration by sensing it at discrete blade surface points, then our perception of vibration severity is additionally dependent on the validity of overall vibratory stress distributions. A digression is needed to consider an approach to establishing fatigue limits in terms of experimental data.

"Operating Limits"—A Function of Mode, Speed, Operating Conditions and Gage Location

The variation of a given sensor's effectiveness, in signaling the severity of vibration at a critical point, is a function of its selected location. It can perhaps best be suggested in terms of what we call "scope limits." A definition of "scope limits" is required. It will be seen that they presuppose the availability of all significant aspects of mean stress, critical point, and blade dynamics.

On-the-spot limits for blade vibration are expressed in terms of strain gage signals as viewed "live" on oscilloscopes. Such limits, because of the manner of observation, we denote as "scope limits," with the implication that vibration at the limit level for a given mode and operating condition represents vibratory stress at the critical point equal to the endurance limit. Relevant rotor speed, inlet pressure and inlet temperature are continuously known, together with readily recognized† blade frequency for selection of the appropriate scope limit established before test. Stress data must be examined for unrestricted service acceptability in the sense symbolized by

$$\%\sigma_a = 100\ \sigma_{v,cp}/\sigma_{a,cp}$$

and in the context of service complications such as foreign object damage.

A scope limit may be defined as

$$\sigma_{sc} = \frac{2\sigma_{a,cp}}{K_v \cdot K_e}\frac{\sigma_{CP}}{E\epsilon_\theta} \qquad (2)$$

where $\sigma_{a,cp}$ is the stress range diagram endurance stress (normally expressed as single amplitude) for the critical point under the given operating conditions, $(\sigma_{cp}/E\epsilon_\theta)$ is the mode- and rotor speed-dependent ratio of critical point vibratory stress to apparent stress sensed by a strain gage (the gage sensitivity ratio); K_v is an experience-derived factor greater than one, implying the presence of a blade in the stage more active than the one directly observed; K_e is a mode frequency-dependent function defining electronic system readout response, normally close to unity. The factor two (2) is introduced to accommodate the natural tendency of electronics technicians to calibrate oscilloscopes in terms of "peak-to-peak" signal levels, avoiding by way of anticipation communication ambiguities. Detailed "mechanics" of application technique will be omitted here, e.g., lab test calibration gage-by-gage, of sensor characteristics; variation of Young's modulus with operating condition-dependent blade temperature, etc. Familiarity with such detailed topics, as well as an adequate understanding of the blade response factor K_v, is presumed and is not critical to the present discussion.

†Presuming adequate pretest blade system dynamics characteristics as a function of rotor speed.

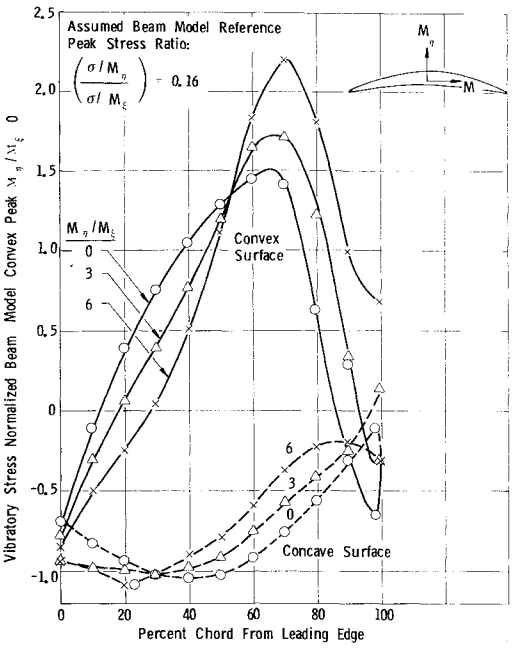

Fig. 12 Blade root vibratory stress distribution—a function of moment ratio M_η/M_ξ. End effects included.

Our interest is restricted here to the manner in which stress distributions affect a) the allowable vibratory stress $\sigma_{a,cp}$, itself dependent on detailed mean stress distributions as we have seen, and b) the innocent-appearing factor $(E\epsilon_\theta/\sigma_{cp})$ dependent on vibratory stress distributions e.g. those of Fig. 12. We may now obtain an indication of the extent to which scope limits (and thereby blade vibration assessment relative to fatigue) are affected by utilization of realistic end effect stress distributions as opposed to elementary, nominal stress distributions.

Consider the effectiveness of strain gage readings in three locations as a function of the convex surface stresses at 5%, 50% and 95% chord. Elementary analysis would consider the leading edge as the critical point; end effect stresses, as observed earlier, would identify the critical point on the convex surface point at 70% chord. From Fig. 11 may be deduced the fraction of critical point stress, that is gage sensitivity ratio $(E\epsilon_\theta/\sigma_{cp})$, perceived at three gage locations on the basis of nominal stresses. Corresponding values of the gage sensitivity ratio can be obtained for stresses as they realistically exist by reference to Fig. 12. Further, noting normalized mean stresses of Fig. 7, applicable for the two stress models, we may obtain the ratio of scope limits as obtained in a nominal stress basis, to that obtained by consideration of end effect stresses.

Table I provides a summary comparison of these results in the context of the particular illustrative end effect stress distributions of the text. Results are not unique nor do they in any way suggest an upper bound by which a nominal stress approach may be in error. It will be seen that convex edge gage limits in this case can provide limits seriously in error and permitting excessive vibration. By a numerical accident of the data set studied, there is only one condition (trailing-edge gage, with $M_\eta/M_\xi = 6$) for which nominal stress analysis would have given an overly cautious limit. Similarly, by a coincidence of stress distributions studied, the midchord gage provides least error for the ratios of M_η/M_ξ studied. There is no implication that a gage in this location, however familiar, provides a safeguard against deficiencies of background analysis.

Table 1 End effect stress implications for scope limits in terms of illustrative gage locations and modes

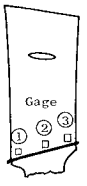

Analysis	Nominal Stress	End Effect Stresses
Critical Point, CP	Leading Edge	70% Chord, Convex Surface
σ_a' Normalized Allowable Vibratory Stress at CP (Ref. Figure 9)	0.82	0.64

GAGE SENSITIVITY RATIO: $E\epsilon_\theta/\sigma_{CP}$

Gage	1	2	3	1	2	3
% Chord	5	50	95	5	50	95
Surface	Convex →			Convex →		
"Mode," M_η/M_ξ						
0	0.42	0.91	0.59	0.26	0.85	0.36
3	0.67	0.64	0.13	0.31	0.70	0.12
6	0.75	0.49	0.13	0.30	0.50	0.35

RATIO OF SCOPE LIMITS: NOMINAL TO END EFFECT BASIS

"Mode," M_η/M_ξ			
0	2	1.4	2.1
3	2.8	1.2	1.4
6	3.1	1.2	0.5

$\dfrac{\sigma_a'\ (E\epsilon_\theta/\sigma_{CP})\ \text{- Nominal}}{\sigma_a'\ (E\epsilon_\theta/\sigma_{CP})\ \text{- End Effect}}$

It may be noted that the gage sensitivity ratio $E\epsilon_\theta/\sigma_{cp}$ actually vanishes for discrete ratios of M_η/M_ζ— specifically at 4.4 for nominal analysis; 3.9, with end effects considered. The reason is apparent from an examination of Figs. 11 and 12, showing that trailing edge stresses change from being in-phase to out-of-phase with critical point stresses as M_η/M increases.

Glimpse of Rotor Speed and Configuration Influence

Expression of scope limits in terms of two vibratory moments, M_ζ and M_η acting on a blade's root section, may be considered a shorthand alert to the need for care in establishing scope limits in an adequate context of rotor speed and overall blade system configuration. There is a natural tendency, for example, to expect that rotor blade scope limits become smaller as rotor speed increases, a "natural tendency" because fatigue endurance limit drops with increasing mean (centrifugal field) stress. But lower-order blade, and blade-disk-shroud system mode stress distributions change as a function of centrifugal field strength, even to the extent that a given sensor's sensitivity ratio ($E\epsilon_\theta/\sigma_{cp}$) may rise faster than endurance limit drops. Scope limits need not drop monotonically with speed; they may rise. Pretest analysis over the whole speed range is, therefore, required even in the context of a single mode to assure that a selected sensor location is consistent with reasonable effectiveness over the whole speed range. Examples may be of interest.

An example is provided by the implications of blade root stress distribution as a function of the moment ratio, M_η/M_ζ in Fig. 12. The blade root section of a part-span shroud blade might be expected to experience a rotor speed variation in the ratio M_η/M_ζ such as that given below to suggest a trend for first blade-disk-shroud system modes of the diametral mode pattern type:

% Rotor speed	0	50	100
M_η/M_ξ	2	4	6

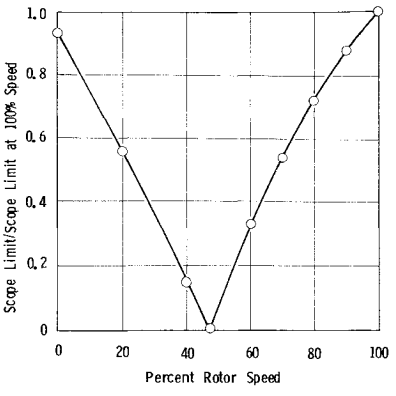

Fig. 13 Illustrative example of scope limit speed dependence for gage location chosen without blade system dynamics consideration.

In a simplified context the mean stress distribution over the blade root cross section of Fig. 12 remains fixed and the reference P/A stress varies with the rotor speed to the second power. Then a gage on the blade root convex surface at 95% chord would experience a large variation in sensitivity ratio ($E\epsilon_\theta/\sigma_{cp}$) while critical point endurance stress would decrease:

Percent rotor speed	0	60	100
Normalized mean stress	0	0.68	1.9
Normalized endurance stress	1.0	0.88	0.64
Sensitivity ratio $E\epsilon_\theta/\sigma_{cp}$	−0.21	0.08	0.35

In relation to its scope limit for 100% rotor speed, the part-speed scope limit for this particular blade would vary, as shown in Fig. 13, wildly and ineffectively.

II. Blade Vibration Design Verification Under Flight Conditions: "Worst Operating Point" Identification

Massive airbreathing engine test facilities at Government installations and throughout the industry testify to foresight in the advantages of engine demonstration at simulated flight conditions. Benefits have accrued to fan and compressor performance, inlet compatibility, and the remedy of blade vibration difficulties frequently deriving more from prior lack of precision in environment definition than from blade characteristics per se. The complexity of this latter design challenge probably precludes our ever dispensing entirely with the need for such demonstrations or discretely defined flight tests.

Illustrative Worst Operating Conditions: Cantilever Stator—Separated Flow and Resonance

Simply by way of illustrating an approach to the process of interpolating among a grid of demonstrations, consider the case of stator vane in a front stage of a multistage compressor known to experience at sea level static conditions a characteristic separated flow vibration at 80% corrected speed; and at 90% rated speed a mechanically excited resonance of modest intensity not significant in itself at, say, 10% fatigue endurance level. Such characteristics are shown in Fig. 14a. Given blade fatigue characteristics of Fig. 14b and a time-average bending stress of 25000 psi at rated sea level conditions, we should be able to predict severity of vane vibration in the two mechanisms noted as a function of inlet pressure (P_{T2c}) and temperature (T_{T2c}) and rotor speed, implicity in terms of flight altitude, plane Mach number, and rotor rpm.

In the restricted sense of combined separated flow vibration and mechanical load resonance, both types involving the same mode of vibration and fatigue critical point,

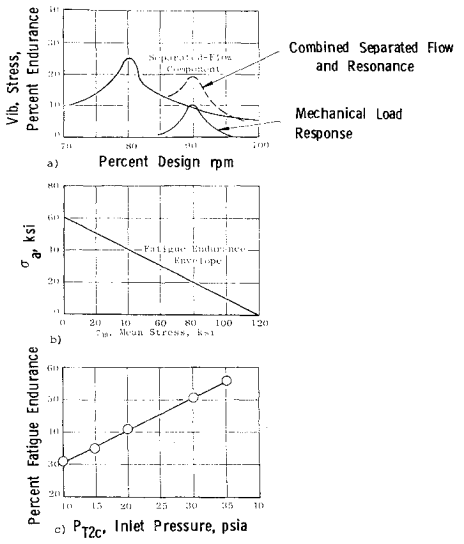

Fig. 14 Illustrative "worst operating point" set for an assumed stator vane. a) Assumed stator vibration at standard atmosphere inlet conditions. b) Assumed stress range diagram. c) Stator vibration variation with inlet pressure at 90% design rotor speed and critical inlet temperature 196°F.

we find that the "worst operating point" vibration will be found at 90% design rpm, a discrete total inlet temperature, 196° F (the critical resonance temperature where the two types of vibration superpose), and at the maximum inlet pressure P_{T2c}. Indeed, recognizing that time average vane stress varies directly as inlet pressure at a given corrected speed, with separated flow vibratory response reasonably forecast as in Sec. 5 of Ref. 5, and assuming such variables as inlet distortion, compressor operating line, and vane damping unchanged from sea level static conditions, one may forecast flight "worst operating conditions" vibration as shown in Fig. 14c.

In a less restrictive sense, blade vibration characteristics noted in Table 2, emphasizing multistage compressors, which experience some complexities of operation absent in fans, suggest that an operating point "worst" for stable vibration is characterized by a combination of variables such as the following: a) critical resonance temperature, T_{2c}; b) maximum consistent P_{T2c}; c) high operating line: realistic equivalent of low-tolerance turbine area and acceleration bias; d) stator schedule—open bias within realistic tolerance (or equivalent aerodynamic stage matching); and e) *realistic*, maximum intensity tip radial distortion pattern operationally consistent with (a) and (b) and containing circumferential component of angular extent containing strongest "per rev" content equal to the blade per rev resonance associated with the "critical resonance temperature" of item (a).

Such a "worst operating point" identification must be realistic in the sense that item conditions above must be consistent. In considerable measure worst operating points can thus be identified in "real world" conditions from unreal, excessive vibration resulting from inlet pressure, inlet temperature, and distortion conditions unsustainable in the actual engine/plane application being investigated; e.g., actual flight idle rpm may keep the rpm for peak separated flow vibration above an rpm at which an inlet distortion resonance may occur. Similar considerations are necessary to provide minimum-risk sequencing of simulated flight tests.

Table 2 Abbreviated classification of compressor operating conditions

Class and subclass	Illustrative trends of vibration
1) Engine mode	
a) Operating line vs steady state, nominal: throttle "burst"/"chop" transients; afterburner transients/controls	High path accentuates front stage vibration. Generally "bursts" mean high line; speed chop, low line. Stall margin design requirements tend to limit operating line excursions.
b) Stator schedule/tolerance transient lag/control malfunction	Open side accentuates front-end, part-speed vib; closed, may accentuate middle stage vibration.
c) Bleed: "customer" bleed/engine cooling	Reduction vs "normal" accentuates front end vibration, excess may increase aft stage vibration.
d) Idle corrected speed: sea level static vs flight	Implications for rpm-dependent resonance.
2) Environment	
a) Distortion—internal fan—transition duct, radial profile temperature, pressure	Tip radial pressure decrement increases front-end part-speed, separated flow vibration; tends to reduce front end stability margin.
b) Distortion—external crosswind:—fan for transport; thrust reverser reingestion emergency stop, fan temperature, pressure, dynamic; supersonic inlet—steady and dynamic	See Ref. 5
3) Flight map	
a) Elevated inlet pressure and temperature superimposed on classes 1 and 2	
b) Significant inlet variables and combinations: temperature	Front-end, part-speed combination of resonance and separated flow vibration, normally absent, are important for very low inlet temperature even at sea level.
inlet pressure	Predictable increase with pressure for separated flow vibration. Similarly, low-order turbine blade resonance. Increased wake-excited resonance. Some decrease in stability margin.
pressure and temperature	As for pressure, above. But note high temperature and related rpm increase introducing some resonances not present at low rpm's.
density and temperature	Max temperature worst for stability margin at part corrected speed, front end stages. Least margin at associated max density.

Blade Instability: Worst Operating Point Identification

Perhaps the most challenging aspect of blade vibration design continues to be to avoid blade instability over all ranges of fan and compressor operation. Verification of instability-free operation is both mandatory and needs to be made with adequate caution. In this context one must consider not only blade stability characteristics as such, but operational complexities in the aero environment in

which they have to be applied; for in some regimes, the challenge of defining aerodynamic parameters of local blade incidence and Mach number, for example, may be greater than of defining stability boundaries expressed in terms of such variables. In the context of realism of operating conditions, a necessary perspective is generally that of verifying blade stability design *margins* with respect to such variables as air relative velocity, incidence angle, and Mach number; and of expressing such margins in terms of variables "directly" measurable, such as inlet T_{T2c}, P_{T2c}, rpm, and stator schedule.

For interest one may list some of the operational variables which could combine to produce a demonstration grid point "worst" with respect to blade instability of the high positive incidence type in a compressor front end stage: a) highest inlet temperature T_{T2c} at intermediate to maximum rotor speed; b) highest inlet pressure for highest inlet density consistent with (a); c) compressor map high operating line, steady state and transient; d) stator schedule, open tolerance, or equivalent stage matching; and e) maximum tip radial distortion, operationally consistent for a given application with (a) through (d).[5]

Flight Map Observations

Requirements for a given engine application include specification of operation within an enclosed area in the flight Mach number/altitude map. The foregoing "worst operating" conditions suggest as most important those flight regimes associated with: a) maximum inlet temperature; b) maximum inlet pressure; 2) maximum density—high Mach flight at low to intermediate altitudes; and d) sea level takeoff in the arctic winter, noting that (e) conditions for flight at "low" Mach number at intermediate to high altitudes may be mcre a question of engine system specifics than primary challenges to blade vibration as such.

Conclusions

1) Experience indicates that systematic experimental verification of blade vibration design relative to fatigue is mandatory for successful airbreathing engine development. It is most effective when regarded as an integral part of the combined aerodynamic and mechanical design process, focusing on validly defined application requirements.

2) The essence of vibration severity assessment consists in increasingly precise and challenging definition of time-average and vibratory stress distributions, point-by-point, throughout blade and support system structures.

3) To the extent that approaches outlined here are carried out in specific detail, deliberate analysis and planning prior to experimental verification permits our knowing what to look for and where, what it means when we have seen it, minimizes risks in "surprise" combinations of operating variables, and provides a priceless opportunity for systematic refinement of our technology base.

References

[1]Danforth, C. E. and Anderson, B. R., "Vibratory Stress Measurements in Multistage Compressor Blading," *Proceedings of the Society for Experimental Stress Analysis,* Vol. XIV, No. 1, 1957, pp. 21–34.

[2]Danforth, C. E., "Designing to Avoid Fatigue in Long Life Engines," *Society of Automotive Engineers Transactions 1967,* Vol. 75, Sec. 2, pp. 248–262.

[3]Beitch, L., "Shell Structures Solved Numerically by Using a Network of Partial Panels," *AIAA Journal,* Vol. 5, March 1967, pp. 418–425.

[4]Chu, C., "The Effect of Initial Twist on Torsional Rigidity of Thin Prismatical Bars and Tubular Members," *1951 Proceedings of the First National Congress of Applied Mechanics.*

[5]Danforth, C. E., "Distortion Induced Vibration in Fan and Compressor Blades," AIAA paper 74-232, Washington, D.C., Jan. 1974.